CASE STUDY

ESPL WILEY

Challenging underground geophysical, geological and topographical surveys in the Borna Maggiore di Pugnetto karst collapse cave to delineate its genesis and actual structure

Cesare Comina[1] [iD] | Michele Motta[1] | Walter Muzzolon[2] | Federico Vagnon[3] | Andrea Vergnano[1]

[1]Department of Earth Sciences, University of Turin, Turin, Italy

[2]Techgea S.r.l, Grugliasco, Turin, Italy

[3]Department of Environment, Land and Infrastructure Engineering, Politecnico di Torino, Turin, Italy

Correspondence
Andrea Vergnano, Department of Earth Sciences, University of Turin, Turin, Italy.
Email: andrea.vergnano@unito.it

Abstract

Electric resistivity surveys in karst environments are commonly employed to establish parameters that can help in the evaluation of collapse risk related to sinkhole or cave formation. However, these surveys are often executed from the surface with consequent limits in resolution and identification potential as a function of coverage thicknesses. Application of these methodologies directly inside known caves, for a better understanding of their formation mechanisms, is uncommon due to accessibility problems, the nontrivial referencing issues that arise when operating in an underground environment and the challenging 2D/3D interpretation issues emerging from the presence of the cavity itself. This paper reports on the application of electric resistivity tomography along with specific geological and topographic mapping, inside the Borna Maggiore di Pugnetto karst collapse cave. Comprehensive knowledge of this cave, developed in mica-rich and carbonate-rich calcschists, is problematic with traditional investigations, due to the cave breakdown that masks its structure. In this study, the 3D geometry of the cave is reconstructed using a topographical survey. This reconstruction is then utilised to perform a 3D inversion of the electrical resistivity tomography (ERT) dataset. The results of both 2D and 3D inversions are compared and discussed, focusing on the survey's ability to identify resistivity anomalies within the 3D volume surrounding the cave. Additionally, an open-source script is provided to facilitate the replication of this 3D modelling and inversion in similar underground contexts. Results of the paper show the effectiveness of the proposed surveys in the delineation of genesis and actual structure of the cave. The paper also proposes a methodological approach that can be adopted in similar contexts to enhance the understanding of speleogenesis.

KEYWORDS
2D/3D electric resistivity tomography, calcschists, cave mapping, collapse caves, karst caves, underground environment

1 | INTRODUCTION

Surface-based geophysical methods can effectively characterise karst environments, complementing traditional geological–structural and topographic surveys (Chalikakis et al., 2011). Geophysical methods are crucial in various applications, such as geotechnical assessments for underground excavations (e.g. Su et al., 2021). They contribute to revealing hidden caves or voids, reducing the potential threats to construction. It is possible to identify weaknesses and develop strategies to mitigate the risk of failures by linking geophysical parameters to

geotechnical ones. Also, hydrogeologists use geophysical methods to identify and monitor aquifers formed in karstic systems (e.g. Song et al., 2020). Additionally, geophysical techniques help identify (paleo) karst formations in oil reservoirs (e.g. (Zhu et al., 2024)), allowing for the assessment of hydraulic continuity, optimization of production and accurate reservoir capacity estimates.

Among the available methods, the use of electrical resistivity tomography (ERT) has considerably increased due to its wide spatial coverage, rapid sampling, low cost, and fast data interpretation compared to traditional geological, hydrogeological, and geomorphological studies (e.g. (Dunscomb & Rehwoldt, 1999; Park et al., 2009)). In an ERT survey, karst voids filled with air are usually detected as resistive anomalies, whereas karst voids filled with fine material or water are observed as conductive anomalies (e.g. Zhu, Currens, & Dinger, 2011). Also, given the increased data distribution and spatial resolution of 3D ERT to rock discontinuities, a 3D acquisition approach can significantly enhance the interpretation of geological features within the host rock structure (e.g. Cheng et al., 2019; Park et al., 2009). Therefore, ERT is commonly applied to detect the presence of caves, given the above depicted contrasts with the host rock. With this respect, ERT has already provided useful results, often in combination with other geophysical methods (e.g. Leucci & De Giorgi, 2005; Martínez-Moreno et al., 2014). Borehole 3D ERTs allowed the creation of 3D models of underground karst systems to assess the stability of the tunnel face (e.g. Bin et al., 2017). Multiple surface ERTs detected and imaged sinkhole phenomena (e.g. Bonetto et al., 2023).

ERT and other geophysical surveys are usually conducted from the surface, which brings a challenge: they generally lose resolution in function of the distance from the source, posing challenges in identifying features inside karst environments. Using geophysical techniques directly in underground areas, preexisting karst cavities or tunnels is less common (e.g. Caselle et al., 2020; Fikos et al., 2021). Moreover, the interpretation of an ERT survey in a cave is not straightforward, and some open questions in the interpretation may arise regarding the role of the cavity itself in the distribution of electrical potential lines. Indeed, the void can strongly influence the electric current flux (air is an insulating material), so a correct interpretation should consider its presence.

Geophysical surveys can, therefore, estimate the distribution of the measured parameter (i.e. resistivity in the case of ERT) potentially correlated to the different materials in the investigated volume. However, the interpretation of geophysical data to reconstruct karst formation and the actual structure of karst cavities is not straightforward and must be performed in combination with detailed topographic and geological surveys (e.g. Bonetto et al., 2023; Cheng et al., 2019; Park et al., 2009).

In this work, a multidisciplinary approach was adopted to study the Borna Maggiore, a karst collapse cave near Pugnetto, in NW Italian Alps. The Borna Maggiore cave has been well known since at least the late 1800s (Martelli & Vaccarone, 1889) and has been extensively studied by many authors (e.g. Capello, 1955; Mammola et al., 2017; Ramella, 1997), with a particular focus on its faunal biodiversity, especially bats, spiders and endemic invertebrates. This biodiversity is indeed the result of the specific microclimatic conditions within the cave (Motta & Motta, 2015a, 2015b, & 2017) and of the fact that

the cave was not affected by glacial processes during the Pleistocene, because the glacial snout was situated 1 km away from the cave (Motta & Motta, 2014; Motta & Motta, 2024). On the contrary, specific geological surveys inside the cave have not been conducted, even though, from a geological point of view, the Borna Maggiore is unique as one of the few karst caves in calcschist worldwide (e.g. Karmann, Sánchez, & Fairchild, 2001). More detailed information on the geological and geomorphological features within the cave might enable a better understanding of its genesis and overall shape. This information may serve as the starting point for further analyses that have not been undertaken so far, such as a better understanding of its hydrogeological aspects.

For these reasons, traditional geological–structural and topographic surveys were integrated with an unconventional underground ERT profile. The study aims to contribute to the reconstruction of cave volumes and the determination of the discontinuity orientations that influence the stability of the rock walls above the cave. Moreover, this survey aims to confirm the hypotheses related to the genesis of the cave and its hydrogeology.

2 | SITE LOCATION AND GEOLOGICAL SETTINGS

The Pugnetto karst system (Figure 1a) is located in the Mezzenile municipality, in the central sector of the Lanzo Valley, 50 km in NW direction from Turin (NW Italian Alps). The Pugnetto karst system comprises four caves (Figure 1a): the Borna Maggiore (820 m above sea level. [a.s.l.]), the Tana del Lupo or Lower Pugnetto Cave (813 m a.s.l.), the Creusa d'le Tampe or Upper Pugnetto Cave (870 m a.s.l.) and the Tana della Volpe Cave (885 m a.s.l.). This study focuses only on the Borna Maggiore cave, the largest of the various caves. The Borna Maggiore has indeed a total planimetric development of 765 m (mapped by the Gruppo Speleologico Piemontese; Balbiano d'Aramengo, 1993).

From a geological point of view, the study area is located at the boundary between the Pennidic domain and the Sesia-Lanzo Unit. The Pennidic domain consists of the pre-Triassic crystalline basement, characterized by polymetamorphism, and the Mesozoic cover (Piedmontese Zone), which has also undergone partial metamorphism. The basement and cover exhibit distinct mechanical properties, resulting in one or more detachment levels; typically, these lithological entities are tectonically independent.

In the Piedmontese Zone, the calcschists and ophiolites (green rocks) represent the evolutionary result of the entire Piedmontese ophiolitic basin, involved and sutured during the collision between the African and European plates. The outcome of this suture, known as the Piedmontese Fold-and-Thrust Belt, exhibits a composite character and is divided into multiple tectonic units, displaying clearly diversified Alpine metamorphic associations and ultimately revealing significant variations in the lithostratigraphic framework. An ancient massif is situated at the inner margin of the Piedmontese Zone, almost devoid of sedimentary cover. Petrographically, the massif consists of two currently juxtaposed units: the Eclogitic Micaschists composed of garnet, Na-pyroxene and blue amphibole, with intercalations of eclogites,
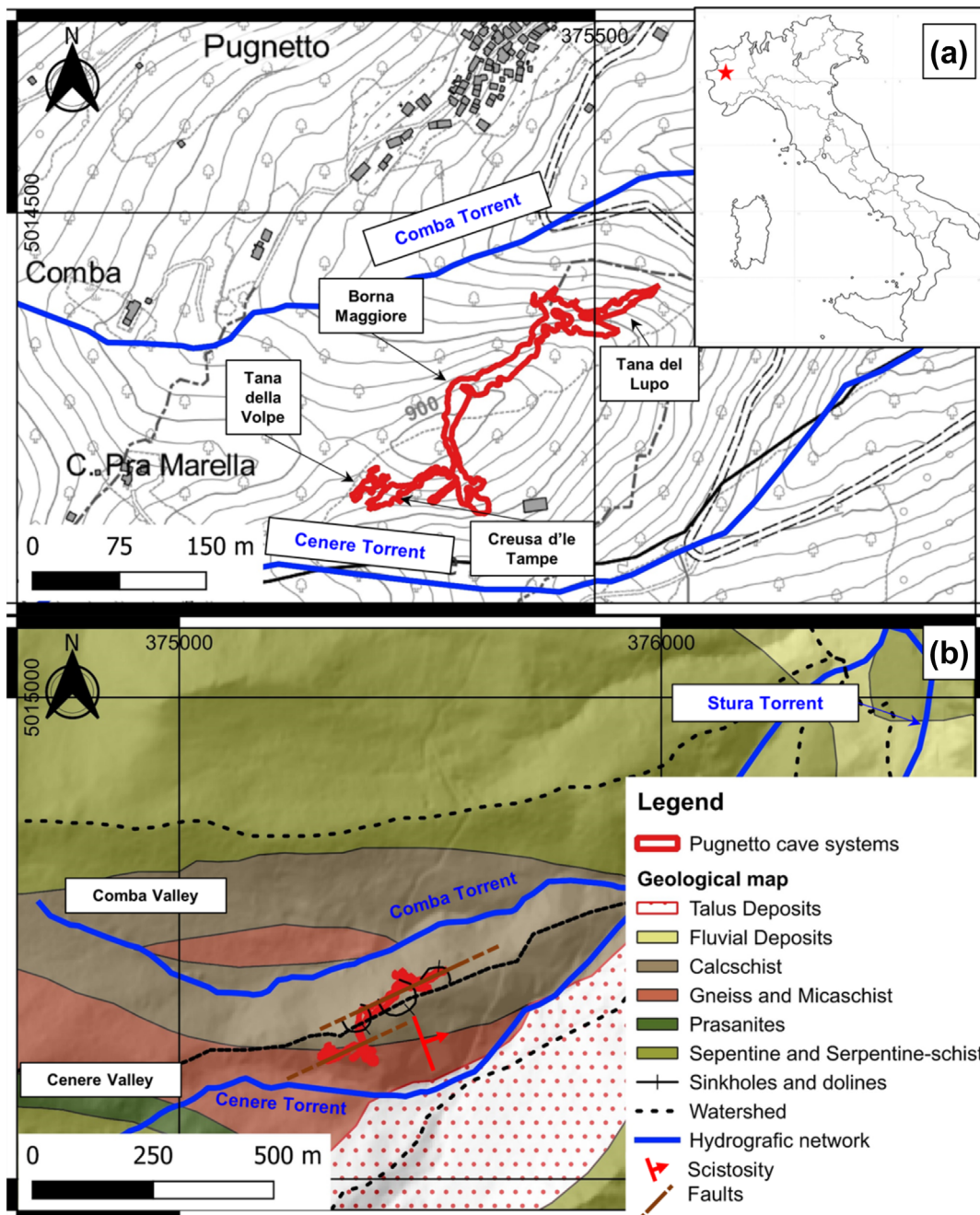
FIGURE 1 (a) location of the test site and (b) sketch of the geological map (Italian Geological Map at the scale 1:100 000—Foglio 55 - CRS: WGS84/UTM zone 32N – EPGS 32632).

glaucophanites and cipollini gneisses, and the complex of 'Gneiss Minuti' (paragneisses).

In this regional geological context, the cave system extends into a lens of mica-rich and carbonate-rich calcschist, sandwiched inside insoluble rocks: gneisses, prasinites and serpentinites (Figure 1b). Karst caves within calcschist are uncommon; consequently, the Borna Maggiore cave represents a unique feature in the Alps. Within the calcschists, the dissolution processes created voids, which triggered widespread collapses, along the lines of rock weakness (i.e. joints, faults and schistosity planes), generating the cave system (breakdown process).

Indeed, the Borna Maggiore is a joint-plane cave developed almost horizontally (Motta & Motta, 2015a). However, the genesis of the original cavity (before the breakdown process) is still uncertain. Surface evidence of the cave's collapse is still visible in the morphological features of sinkholes and dolines corresponding to the hill above the Creusa d'le Tampe (Figure 1).

3 | FIELD SURVEYS, DATA ACQUISITION AND PROCESSING

Geological, topographical and geophysical surveys play a prominent role in cave exploration but give rise to several issues, primarily related to logistics, accessibility and challenging underground conditions. The following sections describe the main surveys conducted
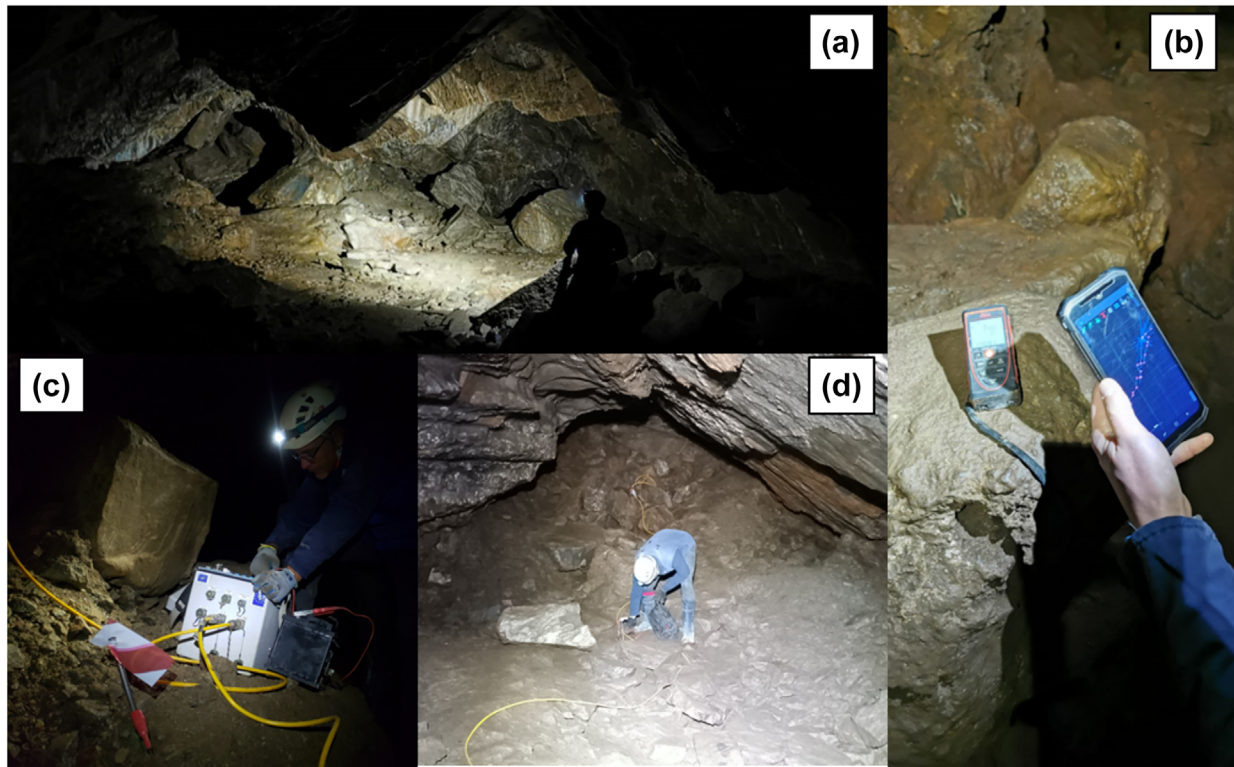
FIGURE 2 (a) Overview of underground environmental conditions at Borna Maggiore and instruments used for (b) topographical and (c–d) geophysical surveys.

within the Borna Maggiore with specific details concerning the strategies adopted to overcome possible difficulties.

3.1 | Topographic survey

Cave mapping can be performed using various techniques: (i) the classical approach tracing a 3D-polyline using tape, compass and clinometer with manual plotting of the results; (ii) a modern approach using portable laser range finders equipped with digital clinometers and compass; and (iii) full 3D and multi-resolution techniques employing total station and/or laser scanner (Ballesteros et al., 2013). Considering their different accuracy and precision, the best choice for a topographical survey might depend on the final requirements, including the size and manageability of the desired results, as well as the environmental conditions in which the survey is conducted (Giordan et al., 2021).

According to Ballesteros et al. (2013), technique (ii) has proven its capability to reproduce good results in terms of accuracy for cave mapping, despite its practicality. This approach was consequently chosen to survey the Borna Maggiore cave. The choice of this topographical methodology allows for a flexible survey due to the presence of narrow paths and the absence of fixed artificial lights, which limited the use of other techniques such as total station, laser scanner or photogrammetric methods.

A modified Leica Disto-X310 (Heeb, 2019a; Heeb, 2019b), combined with the paperless caving system TopoDroid and a differential GPS (Figure 2b), was used for the 3D-reconstruction of the Borna Maggiore cave and the positioning of the geophysical survey within the cave. Details of the instrumentations and the modifications

adopted for the specific working environment of the cave are reported in the supplementary material.

The topographical survey consist of different steps: firstly, a reference point outside the cave was selected and georeferenced using the differential GPS device. Secondly, a polygonal network of reference points was created along the longitudinal axis of the cave (Figure 3a). To correctly georeference the ERT survey, this polygonal network was constructed in correspondence to each measuring electrode (Figure 3b).

Then, for each reference point, Disto-X measurements were taken in all directions to reconstruct the volume of the cavity. Collected data were directly displayed in TopoDroid, for a preliminary visual inspection and potential measurement revision. Lastly, measured data for each point were referenced to a WGS84 UTM 32N reference system.

3.2 | Geological and preliminary hydrogeological surveys

Classical geological survey with a geological compass was conducted within the Borna Maggiore cave in order to map the main geological features, enabling potential interpretations by comparing them with the ERT survey. Additionally, preliminary hydrogeological observations identified the primary water inlets and springs along the cave.

However, the nature of the cave, characterized by confined spaces, limited illumination and uneven terrain (see Figure 2), posed significant challenges for performing geological and geomechanical surveys. Overcoming these obstacles necessitated specialized

FIGURE 3 (a) Reference point outside the cave and polygonal network useful for topographic survey and (b) location of the ERT survey inside the Pugnetto cave system (CRS: WGS84/UTM zone 32N – EPGS 32632). ERT, electrical resistivity tomography.
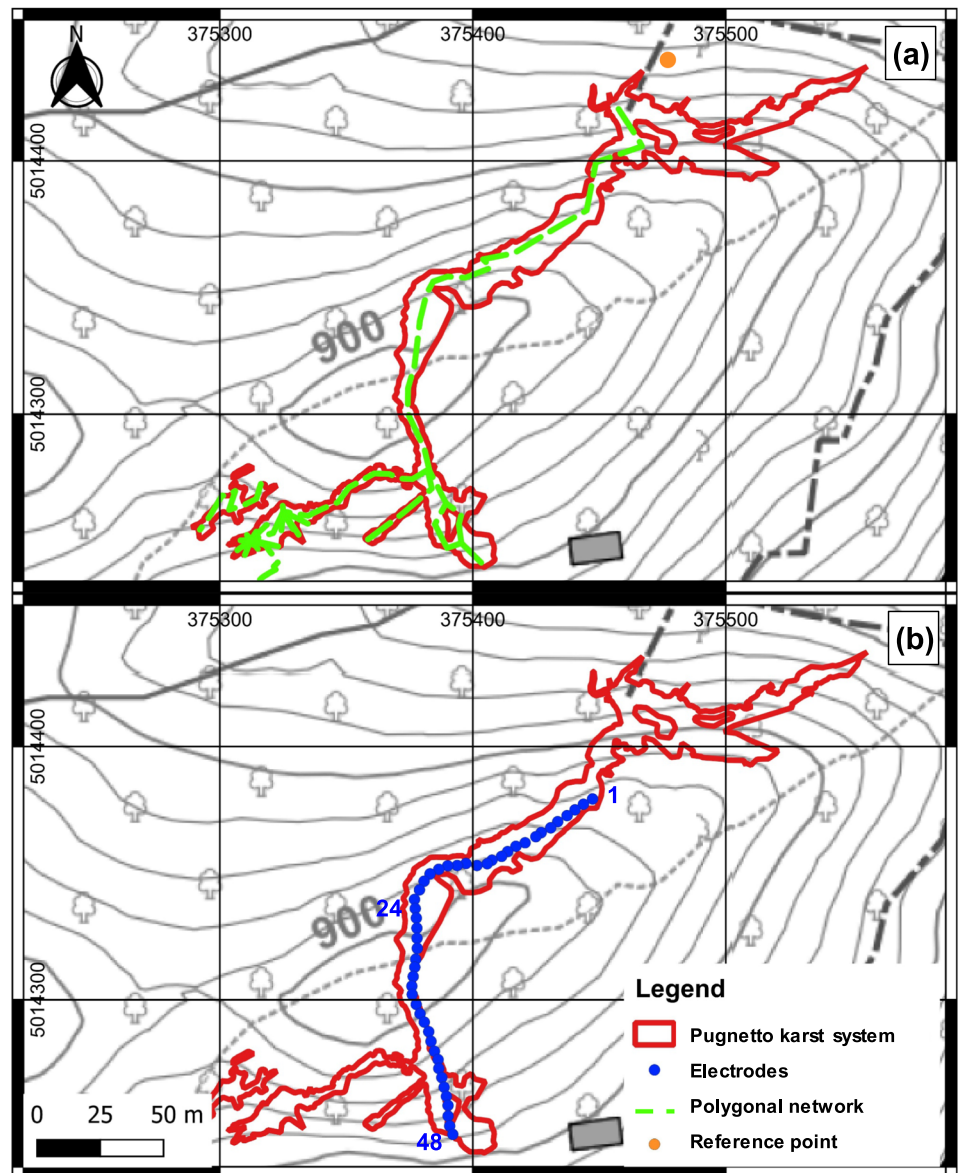
equipment and techniques specifically tailored to the unique conditions of subterranean settings.

3.3 | Geophysical survey—ERT

A 188-m-long ERT was performed by positioning 48 steel electrodes spaced 4 m apart along the longitudinal axis of the Borna Maggiore cave (Figure 3b). Some of these electrodes required the use of a rock drill to be properly inserted and electrically coupled with the rock surface. The Pugnetto cave complex is a SCI (Site of Community Interest), that is, an area protected by strict habitat and biodiversity protection regulations. Consequently, to perform the geophysical survey, it was necessary to request a compatibility assessment from the management authority of Royal Parks protected areas, which subsequently approved this request. Geophysical surveys were therefore carried out at a moment of the year not corresponding to the hibernation period of bats. A georesistivimeter (Syscal Pro by IRIS instruments; Figure 2c) was adopted for the surveys with an acquisition sequence based on dipole–dipole quadrupoles, totalling 497 potential readings. Measurements were repeated on the same quadrupoles with

current and voltage electrodes inverted (i.e. reciprocal data) to evaluate data error. A current injection time of 250 ms was adopted for the surveys. A resistivity check was performed to ensure good coupling between the electrodes and the ground (i.e. contact resistances check). Most of the observed contact resistances were around 5 kΩ, with some slightly exceeding 10 kΩ. Each measurement was repeated at least 3 times, up to a maximum of 6, and the results were stacked, with an accepted error percentage of 5%.

Postprocessing of the acquired data was initially carried out using the ProsysIII software (IRIS instruments) by filtering raw data to eliminate outliers (very high or very low resistivity and isolated) and negative apparent resistivity values. The latter could be, in principle, still present when the resistivity contrast between the conductive body and background medium is extraordinarily high and in near-miss situations, where one of the current electrodes is placed very close to the anomalous body (e.g. Lee & Cho, 2020). However, specific modelling would be required to account for them; the most common approach is instead removing them. Moreover, from the data analysis, the distribution of negative apparent resistivity values appears to be more related to measuring errors than to a specific geological condition. After this preliminary filtering, the data were imported into ResIPy

software (Blanchy et al., 2020). A power-law error model was generated based on reciprocal measurements. This error model, a function of resistance, was used in the inversion to allow measured data to vary within the error range, thereby enhancing the fitting between the measured and calculated models.

To assess the quality, compare potentially obtained results and better understand the distribution of current lines, both 2D and 3D inversions of the acquired data were conducted. Indeed, as shown in Figure 3b, the alignment of the electrodes is not entirely straight and is constrained by the shape of the investigated cavity. Therefore, 3D effects may be present in the data; they could also be due to the presence of the cavity itself. We are conscious that a real 3D inversion, aimed at obtaining a reliable 3D model, would require more survey lines above the cave or around it to constrain the spatial resistivity distribution better. However, the logistical constraints at the site do not allow an easy execution of several survey lines due to (a) the significant topography of the ground surface, (b) the depth of the cave (on average around 40 m) and (c) the fact that the
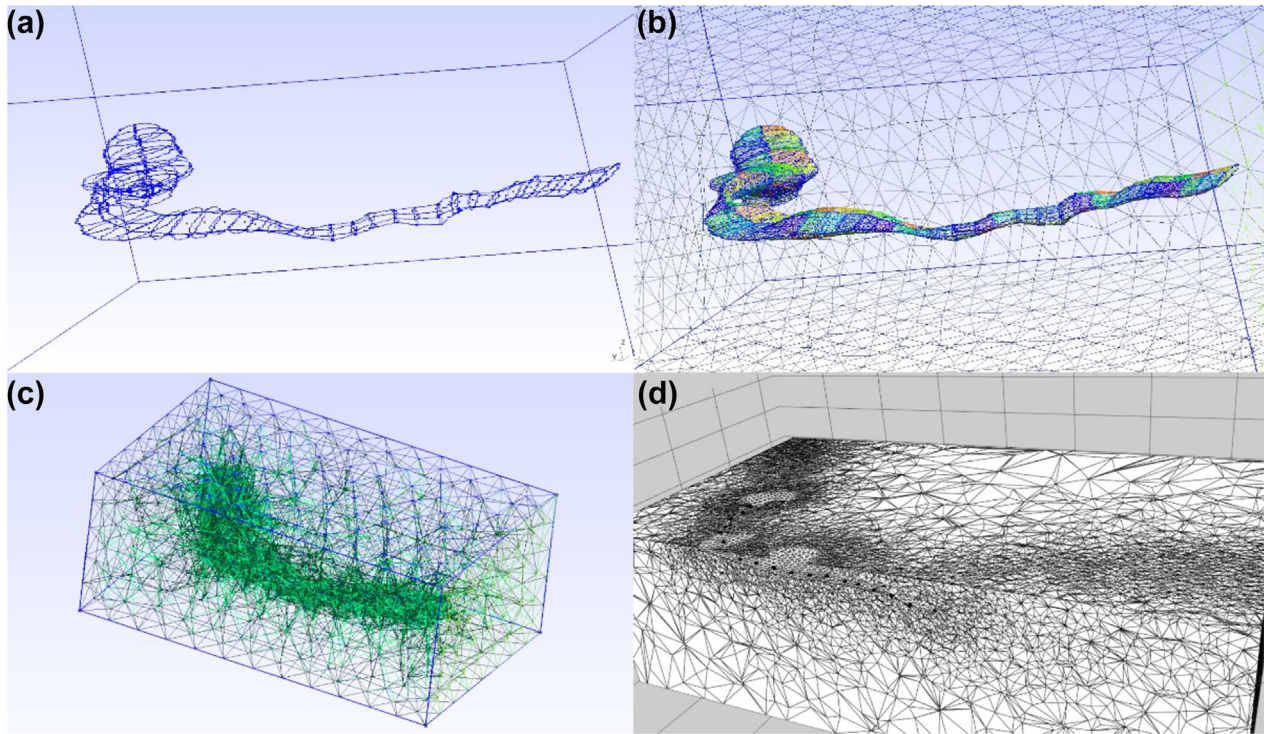

FIGURE 4 The construction of the cave mesh in Gmsh. (a) Cave geometry before meshing. (b) 2D mesh of the cave volume. (c) 3D mesh of the cave volume. (d) 3D mesh imported in ResIPy.
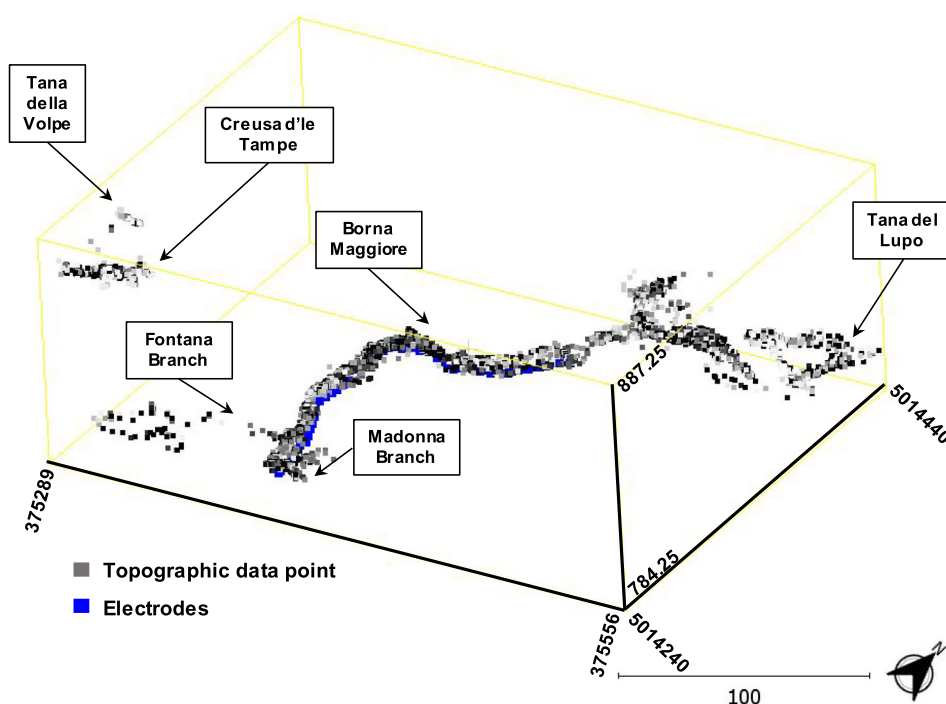

FIGURE 5 Point cloud generated after topographical survey (CRS: WGS84/UTM zone 32N – EPGS 32632).

ground surface is highly vegetated and covered by extensive and dense woodland.

The elaboration of the 3D model from a single line can face challenges in detecting the spatial distribution of resistive or conductive anomalies. The different inversions were, however, performed to discuss the results that could be obtained in similar caves. Indeed, the limitations of our test site could be similar in other contexts, and when the only option is to execute a single survey line, it is important to evaluate the quality of the results and understand their reliability.

For the 2D inversion, even if it would be in principle necessary to calculate the correct spatial distances of the electrodes and use the correct geometrical factors (indeed attempted but not resulting in significantly different results), only the topography was accounted for in the model, and the alignment of the electrodes was considered straight. This approach, albeit not rigorous, was adopted to evaluate potential errors related to neglecting 3D current flux. For this inversion, the characteristic length of the mesh, directly created in ResIPy, was set to be 1 m near the electrodes, and the cell size varied with depth, with a growth factor of 4.

Instead, to perform the 3D inversion, two different approaches were adopted: the first approach ('bottom' 3D) considered only the 3D rock volume below the survey line. The second approach ('full' 3D) considered the whole rock volume (i.e. below and above the survey line) and the presence of the cavity itself. For the 'bottom' 3D approach, the electrodes were considered in their real x, y, z coordinates, and the mesh was created similarly to the 2D inversion for the whole rock volume underlying the electrodes: the characteristic length of the mesh was set to 1 m, and the cell size varied with
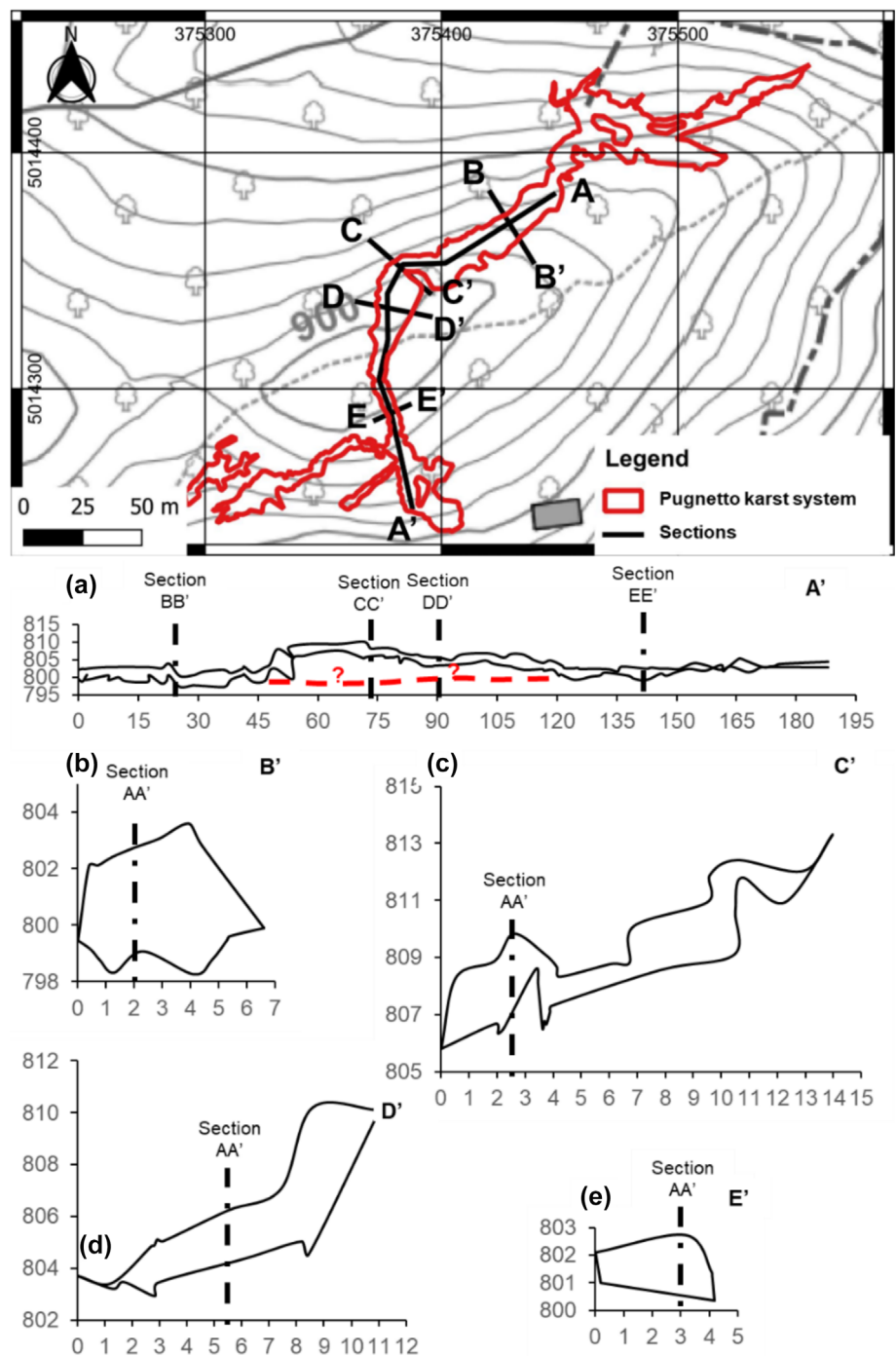

FIGURE 6 Longitudinal and transversal sections along Borna Maggiore Cave (CRS: WGS84/UTM zone 32N – EPGS 32632). Horizontal and vertical distances are in meters.

depth and surface distance, with growth factors of 5 and 8 respectively. For the 'full' 3D approach, a complete 3D mesh, including the cavity itself, was conversely needed. The ResIPy software can create 3D meshes for simple geometries, but the complex geometry of a cave is not among the offered possibilities. Fortunately, because ResIPy can import meshes created with other software, to this end, the open-source mesh creator Gmsh, version 4.12 (Geuzaine & Remacle, 2009), was adopted.

In Gmsh, a 3D mesh with an element size equal to 1 m within the 3 m around the cave surface was defined (Figure 4). The element size dimension linearly decreased with distance from the cave surface, reaching 8 m at a 30-m distance. This choice produced a slightly coarser mesh than the former ones, as a compromise between resolution and computational costs.

The procedure employed to create such mesh is summarized in the following:

1. Process the topographical data to retrieve, for each electrode position, an estimated width and height of the cave at that location (Figure 4a);
2. Write a Gmsh script that builds the geometry of the domain, a box-shaped volume with a hole representing the cave (Figure 4b,c). To this aim, a custom R (R Core Team, 2018) script to import the coordinates of the electrodes and write the Gmsh script automatically was employed;

3. Import the obtained mesh in ResIPy ('import custom mesh' option). This mesh accounted only for the rock volume: the void of the cave was not meshed (Figure 4d).

Because this process is not straightforward, the reader interested in reproducing it in similar contexts such as caves, mines or tunnels is suggested to look at the full details reported in the R and Gmsh scripts available in the supplementary material..

Finally, all the inversions were run. Log-data-based, regularized inversions with linear filtering were performed, aiming at obtaining the desired RMS (root-mean-square) misfit of 1, as calculated by ResIPy, with reference to the power-law error model (i.e. average resulting errors around 5% to 10%). In both 2D and 3D cases, the process converged in three iterations. The complete run of the full 3D inversion, the most computationally expensive, took about 15 min on one computational core (Intel i7-10510U, 4.9 GHz). The starting resistivity model was tested for both 2D and 3D cases with three different constant values: 100, 1000 and 10 000 Ohm.m. Also, different error-managing approaches (with fixed percentage values of 2%, 5% and 10%) were attempted to evaluate eventual smoothness effects during inversions. No meaningful differences were seen in the resulting models after convergence. An estimation of the measurement sensitivity was also computed during the inversion as in Binley (2015) and Binley and Kemna (2005). The imaged sensitivity distribution of the
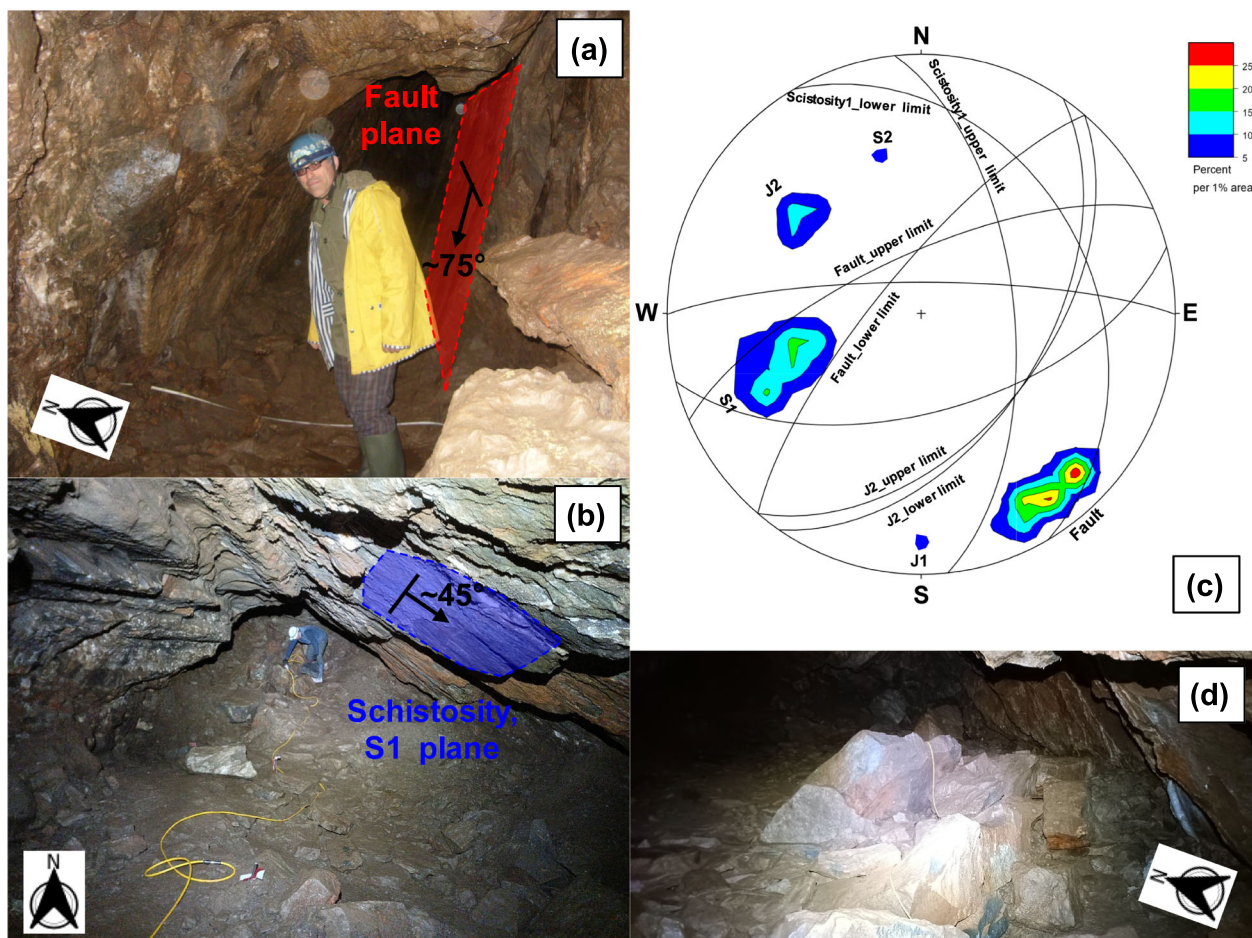

FIGURE 7 (a) Plane of the main fault along which the Borna Maggiore cave developed. (b) Schistosity plane, which determines the cave roof shape. (c) Lower hemisphere Schmidt stereogram summarizing the orientation of the main geological structures surveyed into the Borna Maggiore cave. (d) Shape and volume of rocks fallen from the cave roof.

different performed inversions is a good indicator of the zones of the investigated volume that mostly affect the measured data. Therefore, particularly for 3D inversions, sensitivity distributions can be a useful tool for interpreting the paths of the electric current lines around the cavity. After inversion, the resistivity and sensitivity models were imported into Paraview and CloudCompare software for further visualization and postprocessing.

Also, to better understand the sensitivity limit of 3D inversions and evaluate the reliability of the different investigation zones, specific 3D forward model simulations were performed. The results of these simulations are reported for an example model in the appendix of the paper and in corresponding Figures A1–A5.

4 | RESULTS

4.1 | Topographic surveys

Despite the logistic and access limitations arising from the irregularity of the cave and the presence of lateral branches, a point cloud consisting of 4018 points was generated after performing topographic measurements, as shown in Figure 5. The point density is approximately 1 point each square meter, which can be considered acceptable for this study. Indeed, this point cloud facilitates the 3D reconstruction of the cave, providing valuable information for the geophysical and geological interpretations.

From the imaged point cloud, some considerations on the cave structure can already be performed. Starting from the main entrance, the Borna Maggiore (section AA′ in the Figure 6) gently descends until a small chamber (section BB′ in Figure 6) just before a natural joint (see later J1 in Figure 7), formed by the combination of dissolution effects and subsequent collapse phenomena. At this point, the passage narrows, with a staircase to overcome this constriction and then reach one of the two main chambers of the cave (sections CC′ and DD′ in Figure 6).

From this point, the cave gently descends with a reduced width (section EE′ in Figure 6) to the Cenere Torrent (see Figure 2). Particularly in the vicinity of sections CC′ and DD′, the floor can be walked on highly irregular terrain entirely covered by large irregular blocks (see later Figures 7d and 8b), interspersed with mud and voids. Also, in correspondence with these same sections, the cave is laterally elongated, dipping towards the south. These observations suggest that this portion of the cave could have the greatest amount of collapse blocks. They are indeed visible on the cave floor, and they should reach the base of the original cave void (dashed red line in Figure 6). They also suggest that the shape of the cave in this location is driven by faults and discontinuities inside the rock that originated the collapses. Evidence from the executed geophysical surveys could be helpful in better depicting this contrast.

4.2 | Geological and hydrogeological preliminary survey

The main geological discontinuities along the cave were identified and plotted on the lower hemisphere Schmidt stereogram (Figure 7c). In particular, the following features were observed: (i) fault planes, with plane orientations ranging from 336°/71° to 310°/76° (example in Figure 7a), separating rocks with schistosity planes; (ii) S1 (example in Figure 7b), oriented 60° to 84°/33° to 60° from others with (iii) S2, oriented 165°/59° and joint planes, (iv) J1 oriented 0°/80° and (v) J2, oriented 124° to 130°/50°. These data correspond to the previous structural analysis reported by Motta and Motta (2015a) and contribute to elucidating the genesis of the cave, particularly in areas where cave roofs have experienced collapses and falls. Indeed, the stereogram highlights the possible falling rock blocks with elongated shapes, such as slabs, as well as blocks of cubic shape (see Figure 7d). These blocks form deposits of considerable dimensions and undefined thickness, often filled with finer material, making inspection nearly impossible even for experienced cave explorers.

If compared with hydrogeological and morphological observations, the previous structural analyses suggest that dissolution processes created initial voids (still visible in the Madonna Branch of the) in the more carbonate-rich calcschists (example in Figure 8a). These primordial voids triggered widespread collapse phenomena along the
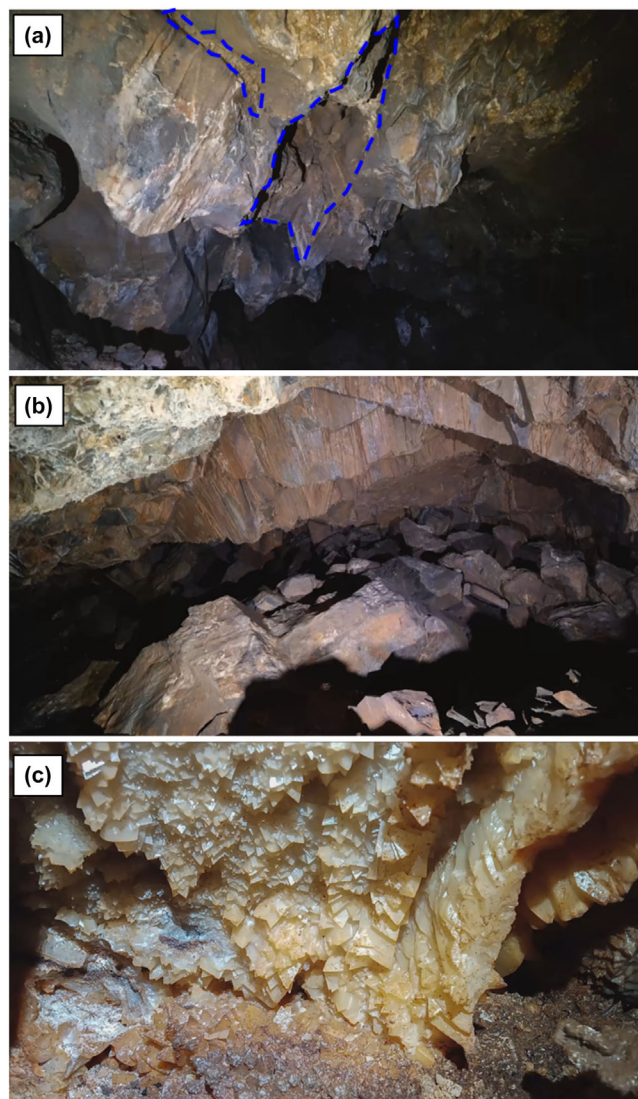

FIGURE 8 (a) Voids in calcschists created by dissolution processes. (b) The typical traces of breakdown processes are striae on the planes of movement (faults and joints) and block deposits. (c) Crystal druses of 'dog's teeth' calcite, crystallized in an underwater environment.
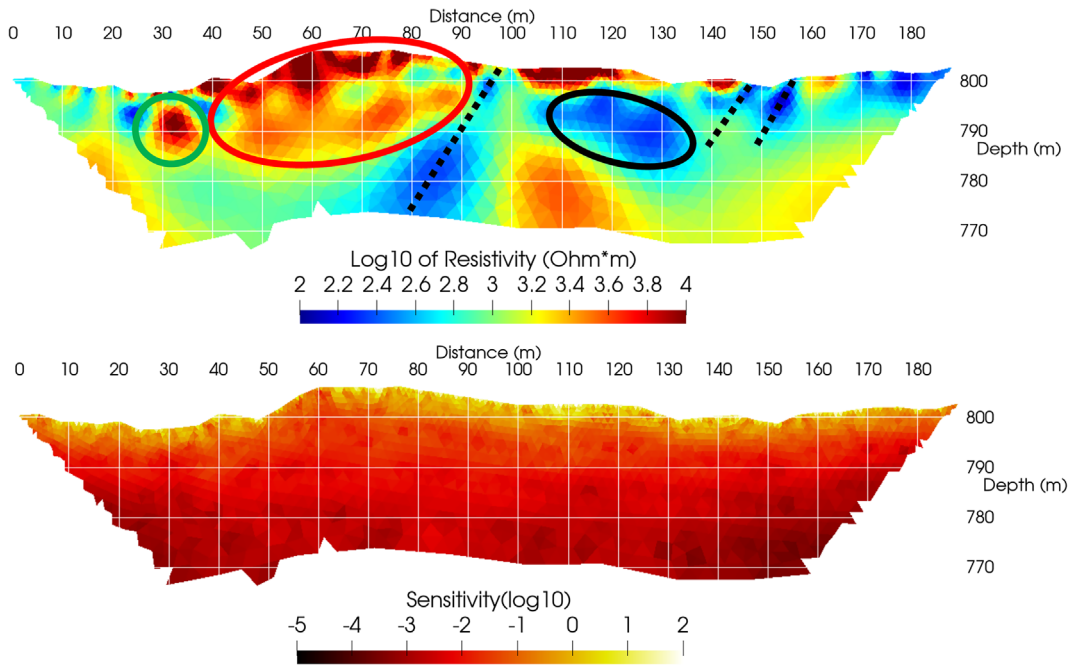
FIGURE 9 2D resistivity model (top) and sensitivity map (bottom) of the rock mass below the cave after 2D inversions. The first electrode, nearest to the cave entrance, is in the left part of the picture.
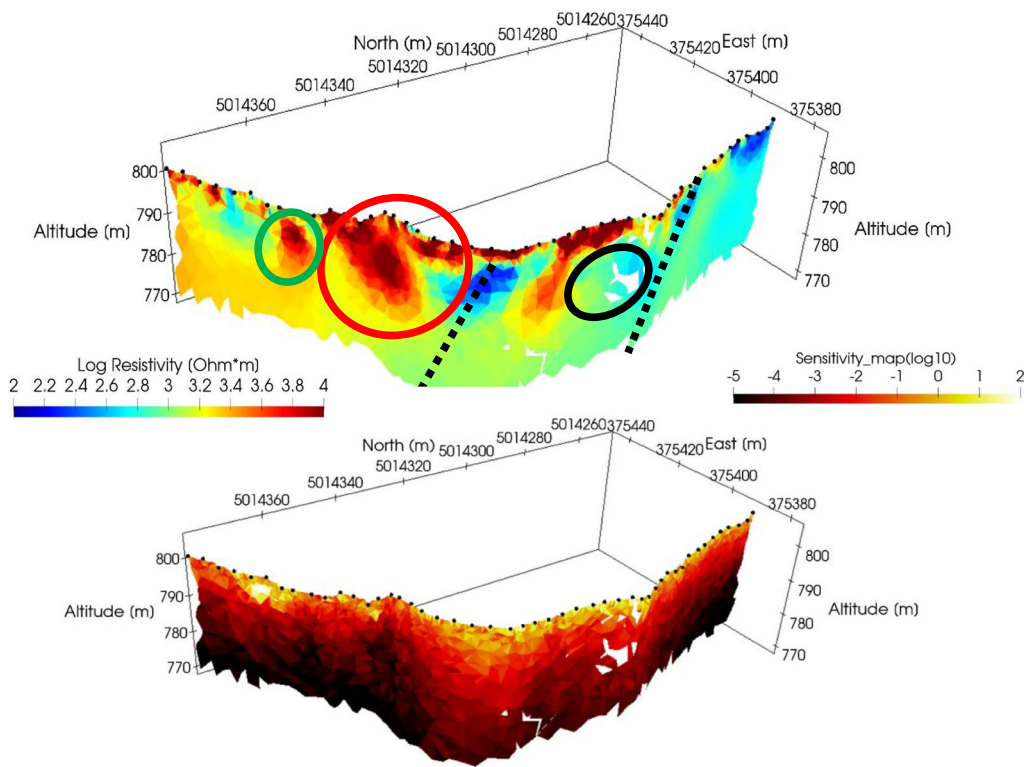

FIGURE 10 The 3D resistivity model (top) and sensitivity map (bottom) with the domain extending only below the cave, vertically sliced in correspondence with the position of the electrodes. The first electrode, nearest to the cave entrance, is in the left part of the picture. Visualization with Paraview (CRS: WGS84/UTM zone 32N – EPGS 32632).

lines of rock weakness (mainly faults and schistosity planes), generating the current configuration of the cave (Figure 8b).

Several crystal druses of 'dog's teeth' calcite, crystallized in an underwater environment, were also observed along the cave (example in Figure 8c) opening interesting suggestions on the phreatic condition of the waters of the cave.

4.3 | Geophysical survey—ERT

The 2D inversion, with topography correction, produced the resistivity model reported in Figure 9. The resistivity model highlights two main resistive areas near the surface, at 40–80 m and 100–120 m from the beginning of the profile respectively. The first of these high

resistivity areas is resistive also at depth (red circle in Figure 9), even with slightly reduced resistivity values. In contrast, in the second area, a low resistivity volume is observed at depth (black circle in Figure 9). An isolated high resistivity anomaly is also observed around 30 m from the beginning of the profile (green circle in Figure 9).

These high resistivity areas can be preliminary related to the presence of big massive blocks below the cave, that is collapsed deposits, and could allow for an estimation of their volume and thickness (see later the discussion section). From about 130 m from the beginning of the profile, surface resistivity appears to be lower, except isolated high resistivity volumes of reduced extension. This is coherent with the second part of the cave being wetter and richer in fine material. Also, the section shows low resistivity bands with consistent orientation (black dotted lines in Figure 9). The orientation of these bands and their relation with the above-described geological survey will be better depicted in the 3D inversion results (see the discussion section). As expected, the model sensitivity decreases with depth, with values below -2 at depths greater than 20 m. From 2D forward model simulations, the -2 sensitivity limit was observed to separate reliable from untrustworthy zones of the model.

The results of the two 3D inversions are presented in the following. The first is the 'bottom' 3D resistivity model obtained considering only the rock volume below the survey line (Figure 10). The second is the 'full' 3D resistivity model extending above and below the cave (with a hole corresponding to the cave volume) coherently with the constructed mesh (Figure 11). They have been sliced along the polyline connecting the electrodes to visualise them properly.

Results obtained with these 3D inversions are consistent with the ones of the 2D inversions. A similar resistivity distribution is observable below the line. For a direct comparison, the same anomalies identified previously are depicted in the figures reporting the 3D results with consistent colour and shape. Of the two 3D models, the one that appears to be more similar to the 2D inversions is the 'full' 3D one. In the 'full' 3D model, it is possible to observe that very low sensitivities are depicted over the cave roof, indicating that most of the current lines are in the volume below the survey line. Also, 3D inversions tend to reduce the magnitude of the resistivity contrast imaged, particularly in the lower resistivity values.

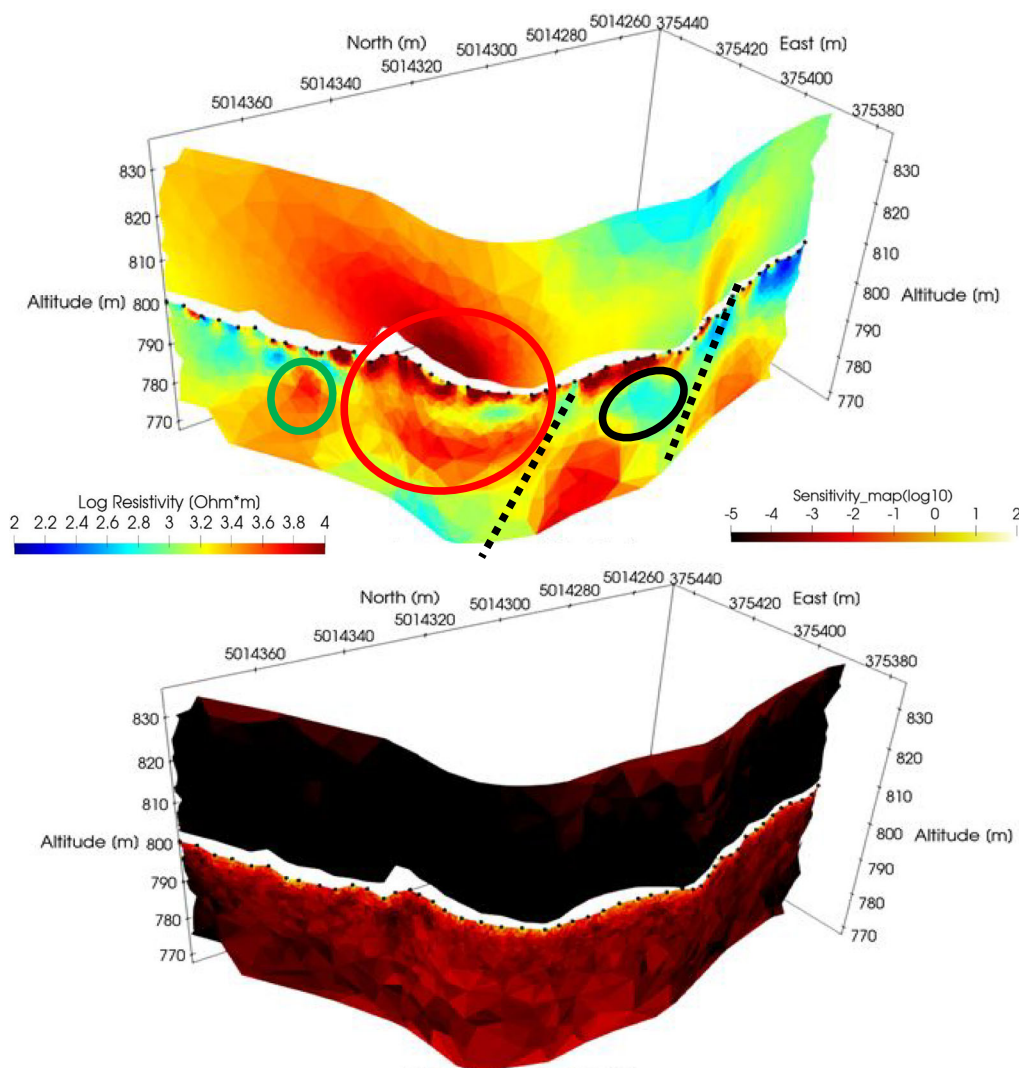The 'full' 3D model was also sliced horizontally at several altitudes (Figure 12).

FIGURE 11 The 3D resistivity model with the cave hole (top) and sensitivity map (bottom), vertically sliced in correspondence of the position of the electrodes. The first electrode, nearest to the cave entrance, is in the left part of the picture. Visualization with Paraview (CRS: WGS84/UTM zone 32N – EPGS 32632).
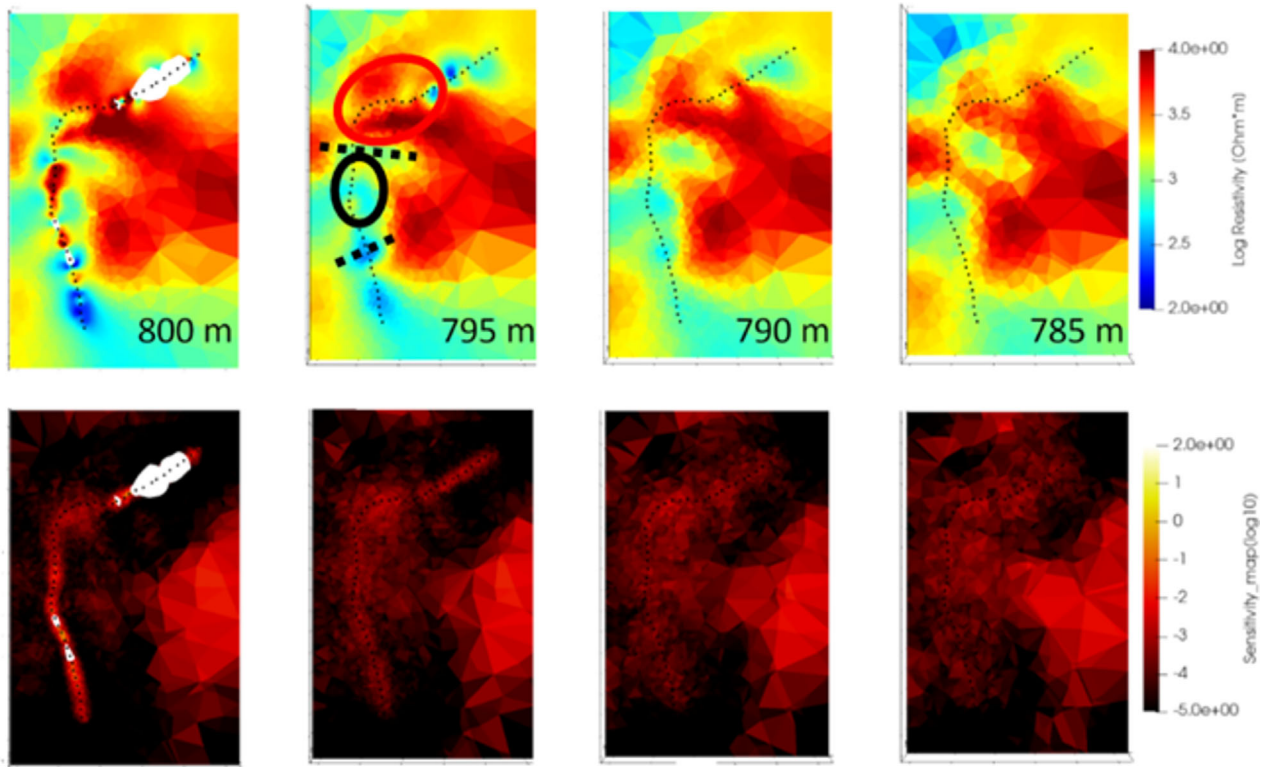
FIGURE 12 The 3D resistivity model (top) and sensitivity map (bottom), horizontally sliced at different altitudes. The first electrode, nearest to the cave entrance, is in the top right part of the picture. Visualization with Paraview (CRS: WGS84/UTM zone 32N – EPGS 32632).
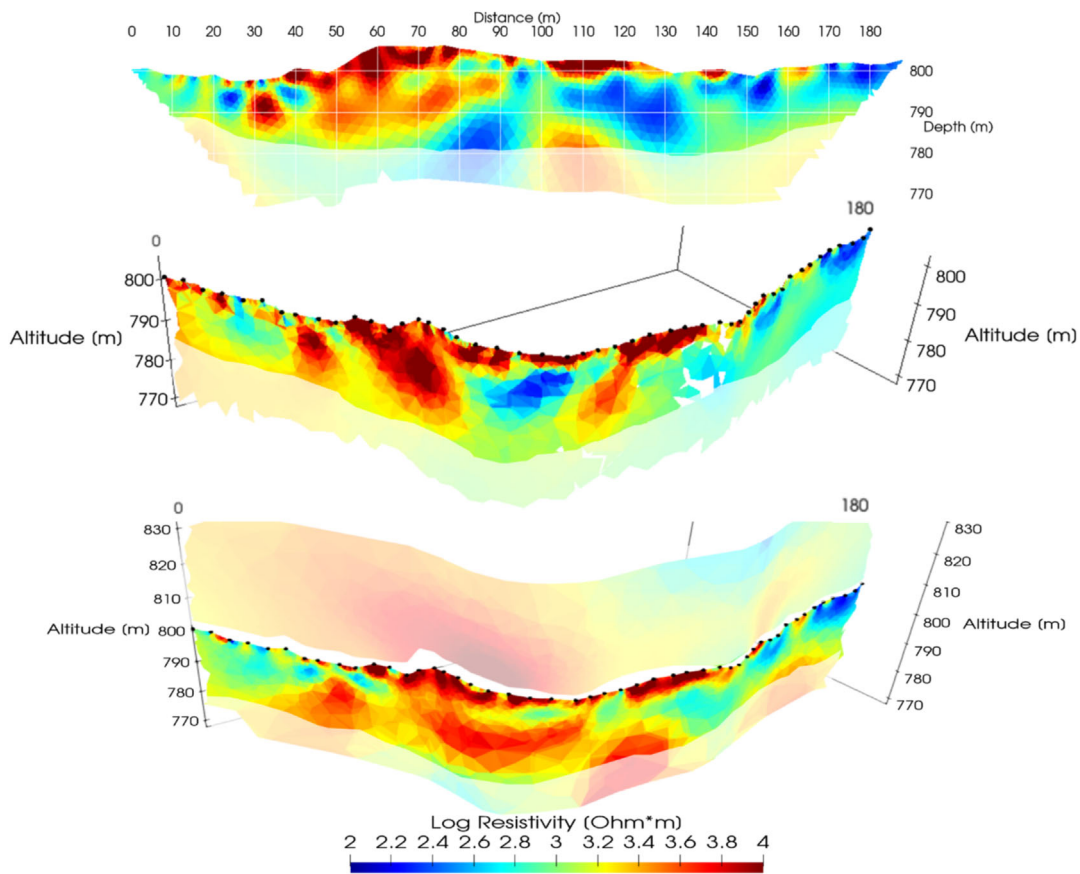
FIGURE 13 The 3D resistivity model of 2D inversion (top), 3D inversion considering only a domain below the electrodes locations (middle) and 3D inversion considering the full domain, above and below the cave (bottom). Visualization with Paraview (CRS: WGS84/UTM zone 32N – EPGS 32632).

In these maps, it is possible to notice how the resistivity and sensitivity distribution vary with depth across the 3D domain. The extracted slices were cut from 800 m a.s.l. (mean elevation of the resistivity profile) to 785 m a.s.l., which corresponds to about 15 m depth. The more conductive layer found in the southern part of the cave extends for less than 10 m, becoming less conductive at depth. In the visualization of Figure 12, anomalies similar to those of Figure 11 are depicted. They are highlighted in the 795 m slice consistently with previous figures.

The sensitivity has high values not only along the line, as expected, but also laterally, especially on the side of the domain towards the centre of curvature of the cave. This suggests that the inversion algorithm rightly considers the horizontal and vertical domains to calculate the resistivity model. In this zone of the model, however, no particular anomalies are depicted, indicating an almost uniform high resistivity volume, reasonably corresponding with the intact rock mass.

The specific 3D forward model simulations (reported in the appendix) allowed us to set a sensitivity limit of about −3 to separate reliable from untrustworthy zones of the model. The forward simulations also highlighted that, despite the limitations of 3D inversions of a single survey line, this ERT configuration can effectively distinguish the 3D location and orientation of certain resistive and conductive anomalies, in both the vertical and horizontal directions.

5 | DISCUSSION

The Borna Maggiore cave develops in a curvilinear shape with variable diameter. The resistivity models produced with the 2D and 3D inversions show that the rocks surrounding the cave are more resistive near the centre of the line, and more conductive at the end of the line.

The goal of comparing a classical, but approximated, 2D inversion with a more consistent 3D inversion was to understand if the 2D model is sufficient to describe the situation of the cave. The cavity itself, or some resistive or conductive blocks not situated below the survey line, may indeed influence the model produced with the 2D inversion. With this respect, a consistent comparison between the results of 2D inversion and both 3D inversions is presented in Figure 13. Coherently with the 2D and 3D forward modelling simulations, the areas with sensitivity below the established reliability thresholds were blanked from the results because they were judged to be untrustworthy.

This comparison shows that, for investigation depths lower than about 10 m, the three models report very similar locations of resistive or conductive areas, as already commented above. However, below 10 m, there are a few differences. In particular, the 2D and the 'full' 3D models are more similar (let aside the mesh size, which is coarser for the 3D case because of the higher computational cost). In contrast, the 'bottom' 3D model provides a partially different interpretation of the three resistive areas in the centre of the picture detected by the other two inversions. This result would suggest that, for this case study of a cave with a certain curvature, the 2D inversion was sufficient to depict the main resistive and conductive anomalies similarly

to the 3D inversion, provided that the 3D model geometry is a good approximation of the reality.

However, the 'full' 3D resistivity model should be considered more representative of the real subsurface resistivity distribution. This model can also be meaningfully cut horizontally, not only vertically, because the rock volume—and therefore the current flow in an ERT survey—extends laterally and vertically in the same way (see Figure 12 of the "Results" section).

In order to ensure a consistent representation of highly resistive volumes, iso-volumes of mesh cells with resistivity > 2500 Ohm.m were computed in Paraview over the 'full' 3D model, among the cells with reliable sensitivity. The distribution of the extracted volumes is reported in Figure 14 and compared to the shape of the cave.

It is evident that most of the high-resistivity cells are located, as expected, in the centre of the line. The total resistive volume extracted was calculated using the 'Python calculator filter' of Paraview and resulted in about 2200 m³. An approximated cave volume for the cave length of the survey is about 4000 m³.

The high resistivity volumes depicted in Figure 14 potentially correspond to the collapsed rock blocks from the cave roof rather than being solely influenced by the void created by the cave's morphometry. This hypothesis is also supported by the observations highlighted in Figure 7. In fact, due to the 3D orientation of the main geological discontinuities (see Figure 7c), the sectors highlighted in Figure 14 also correspond to the sectors that exhibit the most evident roof collapses and irregular block deposits.

The resistivity model obtained through the 3D inversion was visualized together with the main faults and schistosity planes present in the area in Figure 15, where the 'full' 3D resistivity model, sliced
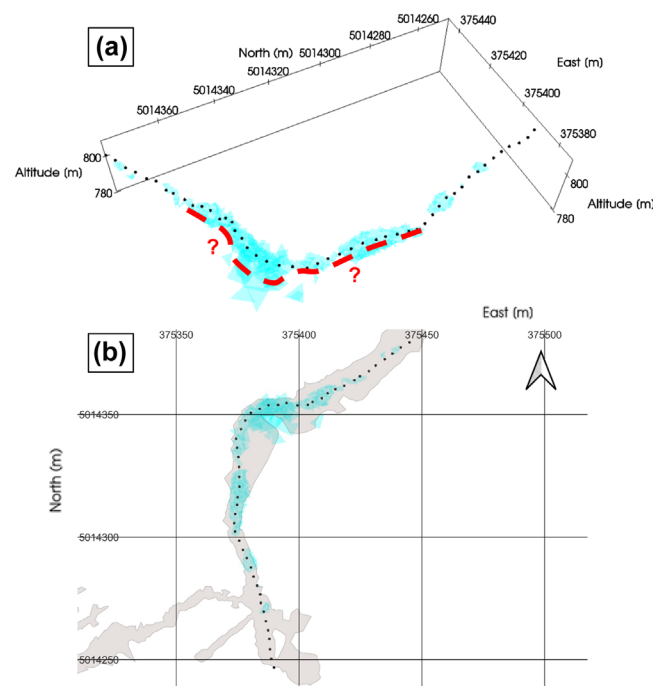

FIGURE 14 Comparison between the resistivity cells > 2500 Ohm.m (extracted among the cells with sensitivity > − 3): (a) 3D visualization and (b) map visualization together with cave volume reconstructed by the points cloud.
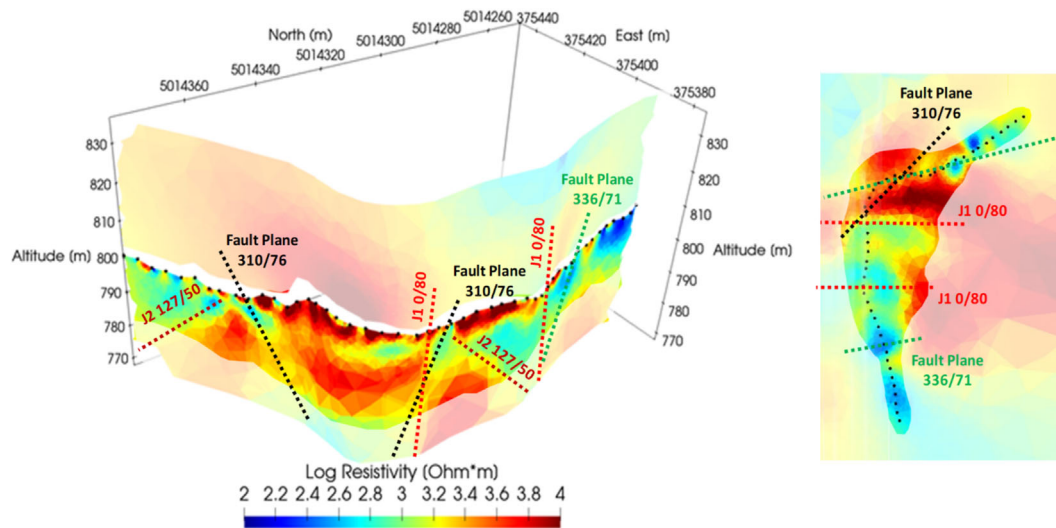
FIGURE 15 Electrical resistivity model, sliced vertically along the electrode line and horizontally at 795 m of altitude, with the main fault, joints and schistosity planes.

vertically along the electrodes line and horizontally at 795 m of altitude, is reported. Again, areas with too low sensitivity are blanked.

This resistivity distribution suggests that some of the elongated resistivity anomalies align well with fault or schistosity planes identified in the geological survey. Additionally, the cave's drainage system significantly affect resistivity, with wetter zones exhibiting higher conductivity compared to the drier, drained zones. The presence of faults, along with the cave itself, modifies the drainage patterns in the rock adjacent to the cave. This often results in one side, where joints, schistosity planes or the fault plane channel water towards the cave, being well-drained and having higher resistivity, in contrast to the opposite side. This effect is clearly illustrated in Figure 15, where the highlighted faults separate rocks with different orientations of the cutting planes, though of the same composition (calcschists).

Also under the cave, the faults influence the resistivity: in the innermost part of the cave (on the right in Figure 15), the fault plane seems to convey the drainage to a low resistivity zone further downstream, 12–15 m below the cave (probably the original tunnel before the cave breakdown).

The high resistivity zone near the surface is, in all probability, the accumulation of blocks of the cave breakdown, whose voids are almost dry. This high resistivity zone is present along almost the entire part of the investigated cave and seems to indicate that the accumulation of blocks from cave breakdown has a fairly limited thickness, around 10 to 15 m.

By merging the geophysical results with the geological evidence, it could be deduced that the karst system drains the waters of the Cenere Torrent (as already hypothesized by Muratore [1925, 1946]), the small valley to the south of the Borna Maggiore, which has a small spring at 800 m a.s.l. (about 20 m upstream of the cave). The waters flow in the karst system and go, without appearing on the surface, to a small valley parallel to the Comba Torrent and further to the north (see Figure 1). This hypothesis is strengthened by the presence of pebbles along the subterranean rivers of the Borna Maggiore, as well as erosion morphologies visible where the collapse of the cave roof has not yet occurred.

In the explored part of the cave, the water initially reaches the Fountain Branch (on the right in Figure 15) and immediately infiltrates the spaces between the blocks accumulated by the cave breakdown (with a discharge generally lower than 1 L/s). Observations of the aquifer level indicate that, from the time of Muratore (Muratore, 1925) to the present day, the water table has significantly lowered. This decrease is attributed not to climate change, but rather to the opening of new drainage routes at lower elevations (Balbiano d'Aramengo, 1993; Massola pers. comm.). The primitive phreatic condition of the cave waters (evidenced by the abundant crystal druses of 'dog's teeth' calcite, crystallized in an underwater environment, Figure 8c) suggests that the external morphology of the area was very different from that of today and that the original cavity formed before the erosion of the underlying Stura Valley at today's altitude (Stura river in Figure 1).

6 | CONCLUSION

The application of ERT, along with specific geological and topographic mapping inside the Borna Maggiore karst collapse cave, provided valuable results and increased our knowledge of the cave structure and potential formation processes. All applied methodologies yielded consistent results along the investigated portions of the cave, revealing similarities related to its structural features.

In particular, the geophysical surveys showed an asymmetry between the portion of the cave near the entrance and its innermost part, which probably reflects a difference in the state of drainage of voids and cracks. This asymmetry would be very little perceptible simply by walking through the cave because the cave appears as an almost horizontal tunnel. Probably, the asymmetry is partly due to more extensive breakdown near the entrance, whereas the end of the cave (the Madonna Branch) retains its original dissolution features. The most plausible explanation is that the voids of the collapse deposits, having a volume far greater than the water runoff, contain mainly air and, therefore, have high resistivity. Perhaps the difference is amplified by geological diversity: The bottom of the Madonna

Branch could be close to the insoluble substrate (consisting of gneiss), which is permeable only by cracking and has its voids in phreatic conditions. The geophysical surveys suggest that the original cave was not horizontal but elongated downhill, probably following the geological contact between soluble (calcschist) and insoluble (gneiss, mica schist) rocks. Therefore, it cannot be ruled out that its waters come from the upper part of the Comba Valley, rather than from the Cenere Valley. Finally, the results indicate that the half of the cave closest to the entrance is the most promising in terms of the possibility of discovering new viable branches.

In conclusion, the performed surveys highlighted the presence of potential cavities and their hydrogeological conditions, showing excellent potential for identifying anomalies for further explorations and research. Moreover, this study also highlights that for caves of this type, characterized by irregular shapes resulting from multiple collapses and moderate presence of water circulation, the influence of the cave void on geophysical interpretations is negligible. Even if this result should be confirmed over different case histories, both classical 2D and fully 3D inversions exhibit clear analogies. Consequently, due to the complexity of survey planning and the computational cost of modelling, 2D inversions appear to be an acceptable solution in this context. Nevertheless, full 3D inversions, even if performed on one survey line, thanks to specific efforts to create the most realistic geometrical model, demonstrated their ability to image off-line structures. Indeed, 3D inversions can provide more comprehensive imaging of the resistivity distribution and allow locating resistive and conductive anomalies in both the vertical and horizontal directions.

DATA AVAILABILITY STATEMENT

The raw and processed data are available in the supplementary materials. The folder contains the following:

1- Raw data in .bin proprietary format and outlier-filtered data in .dat text format, readable by ResIPy and Res2DInv software;

2- Topography data of electrodes and points on the walls of the cave and details of adopted instrumentation;

3- R script, Gmsh script, and mesh .msh file.

4- Inversion folders divided into 2D and 3D, with ResIPy project files (with extension .resipy) and results in .dat and .vtk formats;

5- Paraview folder with .psvm state file and all .vtk and .csv files to recreate that state.

6- Folder with the ResIPy project of the 3D forward simulation described in the appendix, as well as .vtk files readable by for example Paraview software.

The R-script to create the Gmsh script of the 3D cave geometry is also uploaded to GitHub (https://github.com/Andrea-Vergnano/geophysics-utils/tree/main/Mesh_3D_of_a_cave) to allow readers to access updated versions and to modify and improve it.

ORCID

Cesare Comina https://orcid.org/0000-0002-3536-9890

REFERENCES

Balbiano d'Aramengo, C. (1993) Le grotte del Piemonte, A.G.S.P., Via dalla Pazza Folla, Cassolnovo, Italy, p. 183 (in Italian).

Ballesteros, D., Domínguez-Cuesta, M.J., Jiménez-Sánchez, M. & González-Pumariega, P. (2013) Tape-compass-clinometer, DistoX or total station, what is the best method to elaborate a cave survey? A case study in El Pindal Cave, Spain. In Proceedings of the 8th International Conference on Geomorphology, Paris, France, 27–31 August 2013, pp. 27–31.

Bin, L., Zhengyu, L., Shucai, L., Lichao, N., Maoxin, S., Huaifeng, S., et al. (2017) Comprehensive surface geophysical investigation of karst caves ahead of the tunnel face: a case study in the Xiaoheyan section of the water supply project from Songhua River, Jilin, China. *Journal of Applied Geophysics*, 144, 37–49. Available from: https://doi.org/10.1016/j.jappgeo.2017.06.013.

Binley, A. (2015) Tools and techniques: DC electrical methods. In: Schubert, G. (Ed.) *Treatise on geophysics*, 2nd edition, Vol. 11. Amsterdam, Netherlands: Elsevier, pp. 233–259 https://doi.org/10.1016/B978-0-444-53802-4.00192-5.

Binley, A. & Kemna, A. (2005) Electrical methods. In: Rubin, Y. & Hubbard, S.S. (Eds.) *Hydrogeophysics*. Berlin, Germany: Springer, pp. 129–156.

Blanchy, G., Saneiyan, S., Boyd, J., McLachlan, P. & Binley, A. (2020) ResIPy, an intuitive open source software for complex geoelectrical inversion/modelling. *Computers & Geosciences*, 137, 104423. Available from: https://doi.org/10.1016/j.cageo.2020.104423.

Bonetto, S.M.R., Caselle, C., Comina, C. & Vagnon, F. (2023) Geophysical surveys for non-invasive characterization of sinkhole phenomena: a case study of Murisengo. *Earth Surface Processes and Landforms*, 48(9), 1895–1905. Available from: https://doi.org/10.1002/esp.5584.

Capello, C.F. (1955) Il fenomeno carsico in Piemonte. Le zone interne al sistema alpino, C.N.R., Centro studi geografia fisica, Mareggiani, Bologna, ser. 10, vol. 6 (in Italian).

Caselle, C., Bonetto, S., Comina, C. & Stocco, S. (2020) GPR surveys for the prevention of karst risk in underground gypsum quarries. *Tunnelling and Underground Space Technology*, 95, 103137. Available from: https://doi.org/10.1016/j.tust.2019.103137.

Chalikakis, K., Pagnes, V., Guerin, R., Valois, R. & Bosh, F.P. (2011) Contribution of geophysical methods to karst-system exploration: an overview. *Hydrogeology Journal*, 19(6), 1169–1180. Available from: https://doi.org/10.1007/s10040-011-0746-x.

Cheng, Q., Chen, X., Tao, M. & Binley, A. (2019) Characterization of karst structures using quasi-3D electrical resistivity tomography. *Environment and Earth Science*, 78(9), 285. Available from: https://doi.org/10.1007/s12665-019-8284-2.

Dunscomb, M.H. & Rehwoldt, E. (1999) Two-dimensional resistivity profiling; geophysical weapon of choice in karst terrain for engineering applications. In: Beck, B.F., Pettit, A.J. & Herring, J.G. (Eds.) *Hydrogeology and engineering geology of sinkholes and karst*. Rotterdam: Balkema, pp. 219–224.

Fikos, I., Vargemezis, G., Pennos, C. & Tveranger, J. (2021) Contribution of ERT geophysical survey in the study of sediments accumulated inside karstic caves. In: *Proceeding of the 11th congress of the Balkan geophysical society*. Bucharest: European Association of Geoscientists & Engineer, 10–14 October 2021.

Geuzaine, C. & Remacle, J.-F. (2009) Gmsh: a three-dimensional finite element mesh generator with built-in pre- and post-processing facilities. *International Journal for Numerical Methods in Engineering*, 79(11), 1309–1331. Available from: https://doi.org/10.1002/nme.2579.

Giordan, D., Godone, D., Baldo, M., Piras, M., Grasso, N. & Zerbetto, R. (2021) Survey solutions for 3D acquisition and representation of artificial and natural caves. *Applied Sciences*, 11(14), 6482. Available from: https://doi.org/10.3390/app11146482.

Heeb, B. (2019a) Paperless cave surveying. Available at: http://paperless.bheeb.ch/, Accessed 6th May 2024.

Heeb, B. (2019b) DistoX2 hardware information package. Available at: http://paperless.bheeb.ch/download/DistoX2Hardware.zip, Accessed 6th May 2024.

Karmann, I., Sánchez, L.E. & Fairchild, T.R. (2001) Caverna Dos Ecos (Central Brazil): genesis and geomorphologic context of a cave developed in schist, quartzite, and marble. *Journal of Cave and Karst Studies*, 63(1), 41–47.

Lee, K.S. & Cho, I.K. (2020) Negative apparent resistivities in surface resistivity measurements. *Journal of Applied Geophysics*, 176, 104010. Available from: https://doi.org/10.1016/j.jappgeo.2020.104010.

Leucci, G. & De Giorgi, L. (2005) Integrated geophysical surveys to assess the structural conditions of a karstic cave of archaeological importance. *Natural Hazards and Earth System Sciences*, 5(1), 17–22. Available from: https://doi.org/10.5194/nhess-5-17-2005.

Mammola, S., Piano, E., Giachino, P.M. & Isaia, M. (2017) An ecological survey of the invertebrate community at the epigean/hypogean interface. *Subterranean Biology*, 24, 27–52. Available from: https://doi.org/10.3897/subtbiol.24.21585.

Martelli, A. & Vaccarone, L. (1889) *Guida delle Alpi Occidentali*. Milano, Italy: Club Alpino Italiano (in Italian).

Martínez-Moreno, F.J., Galindo-Zaldívar, J., Pedrera, A., Teixido, T., Ruano, P., Peña, J.A., et al. (2014) Integrated geophysical methods for studying the karst system of Gruta de las Maravillas (Aracena, Southwest Spain). *Journal of Applied Geophysics*, 107, 149–162. Available from: https://doi.org/10.1016/j.jappgeo.2014.05.021.

Motta, L. & Motta, M. (2014) Oscillations of temperatures in Piedmont caves remarkable for speleofauna, SCIECONF 2014, EDIS, Zilina, Slovak Republic, pp. 412–417.

Motta, L. & Motta, M. (2015a) The climate of the Borna Maggiore di Pugnetto Cave (Lanzo Valley, Western Italian Alps). *Universal Journal of Geoscience*, 3(3), 90–102. Available from: https://doi.org/10.13189/ujg.2015.030303.

Motta, L. & Motta, M. (2015b) Thermic characterization of the underground superficial compartment near Pugnetto cave system (Lanzo Valley, Western Alps). In: Proceedings of the 4th International Virtual Conference on Advanced Research in Scientific Area (ARSA-2015), Vol. 4, pp. 216–221, Zilina, Slovak Republic.

Motta, M. & Motta, L. (2017) *The climatic study of caves with single entrance*. Raleigh (USA): Lulu, p. 71.

Motta, M. & Motta, L. (2024) Fundamental aspects of the cave microclimate in the environmental quality of Borna Maggiore di Pugnetto S.C.I. (Lanzo Valley, Piedmont). In: Bovo, A., Masciocco, L. & Sassone, P. (Eds.) *Geologia Ambientale in Piemonte e Valle d'Aosta*. Capurso (BA): Sigea, pp. 135–141.

Muratore, G. (1925) Grotte del Pugnetto. Rivista del Club Alpino Italiano 8, pp. 192–197 (in Italian).

Muratore, G. (1946) Grotte del Pugnetto, valli di Lanzo - Stura di Ala. *Rivista Mensile Club Alpino Italiano*, 65(1–2), 21–29. (in Italian).

Park, S.G., Kim, C., Son, J.S., Yi, M.J. & Kim, J.H. (2009) Detection of cavities in a karst area by means of 3D electrical resistivity technique. *Exploration Geophysics*, 40(1), 27–32. Available from: https://doi.org/10.1071/EG08114.

R Core Team. (2018) R: A language and environment for statistical computing. R Foundation for Statistical Computing, Vienna, Austria. Available at: https://www.R-project.org/, Accessed 8th October 2024.

Ramella, L. (1997) Atlas des cavités non calcaires du monde, Union Intérnational de Spéléologie, pp. 68–70 (in French).

Song, K., Yang, G., Wang, F., Liu, J. & Liu, D. (2020) Application of geophysical and hydrogeochemical methods to the protection of drinking groundwater in karst regions. *International Journal of Environmental Research and Public Health*, 17(10), 3627. Available from: https://doi.org/10.3390/ijerph17103627.

Su, M., Zhao, Y., Xue, Y., Wang, P., Xia, T., Zhang, K., et al. (2021) Progressive fine integrated geophysical method for karst detection during subway construction. *Pure and Applied Geophysics*, 178(1), 91–106. Available from: https://doi.org/10.1007/s00024-020-02636-4.

Zhu, D., Xiangwen Li, R.G., Shifan Zhan, L.L., et al. (2024) Paleokarst caves recognition from seismic response simulation to convolutional neural network detection. *Geophysics*, 89(1), 1942–2156. Available from: https://doi.org/10.1190/geo2023-0133.1.

Zhu, J., Currens, J.C. & Dinger, J.S. (2011) Challenges of using electrical resistivity method to locate karst conduits—a field case in the inner bluegrass region Kentucky. *Journal of Applied Geophysics*, 75(3), 523–530. Available from: https://doi.org/10.1016/j.jappgeo.2011.08.009.

SUPPORTING INFORMATION

Additional supporting information can be found online in the Supporting Information section at the end of this article.